An experimental investigation of dynamic behavior in FePt systems

2009 J. Phys.: Condens. Matter 21 124203

(http://iopscience.iop.org/0953-8984/21/12/124203)

J. Phys.: Condens. Matter **21** (2009) 124203 (11pp) doi:10.1088/0953-8984/21/12/124203

An experimental investigation of dynamic behavior in FePt systems

R O Fuller[1,2], G A Koutsantonis[1] and R L Stamps[2]

[1] Chemistry, M313, School of Chemical and Biomedical Sciences, University of Western Australia, 35 Stirling Highway, Crawley WA, 6009, Australia
[2] School of Physics, M013, University of Western Australia, 35 Stirling Highway, Crawley WA, 6009, Australia

E-mail: becky@physics.uwa.edu.au (R O Fuller)

Received 13 September 2008, in final form 5 February 2009
Published 25 February 2009
Online at stacks.iop.org/JPhysCM/21/124203

Abstract
Magnetic relaxation experiments have been used to investigate the non-equilibrium dynamics of FePt nanoparticles. The system exhibits ageing at low temperatures, as well as a narrow energy distribution of the barrier to reversal. These properties were found susceptible to being affected by particle size, matrix and applied field strength. An analysis based on broad rate distributions is presented and compared with results obtained using energy barrier and viscosity interpretations. We find that a single broad distribution of relaxation times suggestive of cooperative effects is sufficient to explain the experimental results.

1. Introduction

Dynamic properties in magnetic nanoparticulate systems have received attention in recent times due to their potential use as magnetic recording media, biomedical sensors and new electronic devices. Properties of nanoparticulates have been reviewed by both Jönsson [1] and Dorman [2]. Nanoparticle assemblies can behave as non-interacting (or very weakly interacting) particles, where dynamic behavior is sensitive to the distribution of energy barriers. Conversely strong interactions between nanoparticles can dramatically effect dynamic properties. For example dipolar interactions between particles can lead to frustration and drive slow dynamics on long timescales [3, 4].

In this paper we present experimental results for single domain nanoparticles. At high temperatures the particles behave as superparamagnets, where the magnetic moment relaxation time is less than the measurement time. As the temperature is lowered the magnetic moments are trapped for long times in one state. Magnetic relaxation measurements on these systems can be used to study dynamic behavior as this governs the region where the spin relaxation time is of the order of the observation time.

Slow dynamic effects such as ageing, memory and cooperative behavior in a range of materials have been studied experimentally [3–6] and theoretically [7–10]. Magnetic viscosity or relaxation is the variation in the magnetization of a system in a constant applied field [11]. Unusual low temperature behavior has been noted in the energy barrier distribution inferred from magnetic viscosity measurements of a number of systems [12–14]. The energy barrier distribution describing relaxation in these reports is comprised of two components, a log normal and an exponential. The log normal component has been attributed [12, 15] to a distribution of barriers. The origin of the exponential component is less clear. It has been postulated [12, 15] that this behavior in ionic magnetic solids and ferritin is the result of magnetic interactions due to surface effects. In contrast Mamiya *et al* [16] suggested this exponential contribution to the distribution does not exist and is an artifact generated by a distribution of particle sizes.

In this work we explore the nature of an apparent exponential contribution to the reversal barrier using types of viscosity measurements interpreted in terms of relaxation time distributions and compared with results from energy barrier analysis. We have extended our initial investigation [13] into the metallic particle system, FePt by synthesis of new samples and performed more extensive magnetic measurements. In particular we investigate to what extent particle surfactant matrix and size govern the thermal relaxation of nanoparticulate systems and can result in anomalous low temperature behavior in both static viscosity and dynamic ageing experiments. Results suggest interparticle interactions, possibly due to a combination of elastic matrix

and dipolar energies, may be the cause of low temperature exponential relaxation. A connection between our activation rates interpretation of the time dependent magnetization and energy barrier/viscosity interpretation is derived theoretically.

2. Experimental details

2.1. Nanoparticle synthesis and characterization

The nanoparticles used for this investigation included a 4 nm $Fe_{20}Pt_{80}$ system whose synthesis and characterization has been [13] previously described. A second 4 nm $Fe_{20}Pt_{80}$ system was made by modifying the surfactant of the original particles. The as-synthesised eighteen carbon backbone surfactants (oleic acid and oleyl amine) of the original particles was replaced with an eight carbon backbone (octanoic acid and octanoic amine) system through a series of centrifugation steps [17]. These samples are denoted as 4C18 and 4C8 respectively in this paper. Samples for transmission electron microscopy (TEM) were prepared by depositing a single drop of dilute FePt ($\sim$1 mg mL^{-1}) on a carbon coated copper grid. The samples consisted generally of a monolayer of particles. Using TEM particle size, purity and interparticle spacings were obtained by manually taking intensity line scans across the particles and setting a suitable threshold intensity value to identify the edges of the particles. 50 particle and 50 interparticle spacings were measured for each sample. The particles were found to be monodispersed with a standard deviation of 7.8%. A small change in interparticle spacing was seen when eight carbon backbone surfactants were used, 2.4 nm compared to the 2.8 nm seen for 4C18. The associated standard deviation also changed from 12.5 to 14.3%. The moderate deviation results from the pixels in the image and the particle threshold limits. Since the difference is greater than 10 pixels, it constitutes a real change in interparticle spacing.

A system of 6 nm $Fe_{27}Pt_{73}$ was synthesized using *in situ* seed mediated growth [17]. A reductive thermal decomposition reaction between $Pt(acac)_2$ and $Fe(CO)_5$ in the presence of oleic acid and oleyl amine under standard Schlenk conditions was used. The composition of the nanoparticle bulk solution was determined through inductively coupled plasma atomic emission spectroscopy. The resultant reaction mixture contained both 3 and 6 nm particles. The larger particles were separated out of the bulk reaction solution by a series of centrifugation steps [17]. The sample used for the magnetic measurements contained more than 95% of the 6 nm particles. These were monodispersed with a standard deviation of 5% and an average interparticle spacing of 3.9 nm (standard deviation $\sim$7.5%). Results were confirmed through TEM, an example is shown in figure 1, and the system will be referred to as 6C18. Larger interparticle spacing allowed more accurate measurements to be made, thereby reducing the standard deviation compared to that of the 4 nm particles. High resolution TEM revealed the single crystal (figure 1) nature of individual particles.

All FePt particles synthesized had an unordered face centered cubic (FCC) phase and a low anisotropic chemical ordering. This was confirmed through x-ray diffraction (XRD) and selected area diffraction (SAD). Samples for XRD were prepared by depositing a hexane dispersion of particles on a glass slide. The solvent was allowed to evaporate and the process was repeated to build up enough sample mass for detection, results were shown to be reproducible. Results are shown in figure 1. Using Bragg's law the lattice parameter, a was calculated from the XRD to be 3.9(1) Å and from SAD the parameter, c was found to be 4.47(3) Å. The small discrepancy in the values is due to the asymmetric nature of the FCC unit cell (i.e. comprised of lattice parameters $a \neq c$) due to the high platinum composition [18]. From Klemmer *et al* [18] one would predict the lattice parameters for 4C18, 4C8 and 6C18 to be $a \sim 3.9$ Å and $c \sim 4.3$ Å, so the values obtained are reasonable. It should be noted that the slight difference of Pt concentration does not greatly effect the lattice parameters at these compositions and it is only important as the system becomes more equiatomic or for Fe saturated compositions [18].

2.2. Magnetic measurements

All magnetic measurements were performed using a Quantum Design MPMS-7 SQUID magnetometer. There were three main types of experiments performed in this work: field cooled (FC) and zero field cooled (ZFC) magnetization as a function of temperature, time independent ZFC magnetic relaxation and FC and ZFC ageing relaxation experiments. Samples were prepared in the same manner as for XRD. It should be noted that magnetic moments cannot be given precisely as moment per particle because the mass of the FePt nanoparticles cannot be determined separately from the surfactant present to stabilize particles.

2.2.1. ZFC and FC magnetization as a function of temperature. ZFC and FC (1000 Oe) magnetizations were measured as a function of temperature (5–350 K) in a 10 Oe field on all samples. This gives a measure of the blocking temperature, T_B where the system goes from an unordered superparamagnetic to an ordered ferromagnetic state.

The full results for 4C18 are shown in figure 2 as well as the blocking region for 4C8 and 6C18. All particle systems were found to exhibit typical nanoparticle superparamagnetic behavior at high temperatures. At low temperatures the ZFC and FC magnetization curves differ. The ZFC curve has a maximum near T_B, while the FC curve continues to increase as temperature decreases. This is seen in figure 2(a) for 4C18 and figure 2(b) for 4C8 and 6C18. T_B for 4C18 and 4C8 was found to be between 20 and 30 K. While for 6C18, T_B was between 35 and 45 K.

2.2.2. ZFC magnetic viscosity. The time dependent magnetic relaxation was measured by cooling the sample from above T_B (in zero field) to a desired temperature (2–30 K for 4C18/8 and 2–50 K for 6C18). An average moment was then created by applying a field of 7 T. The field was then removed stepwise and the superconducting magnet quenched to ensure any trapped flux was removed. Magnetization data was then collected for the next 1700 s at 20–50 s intervals. For this and

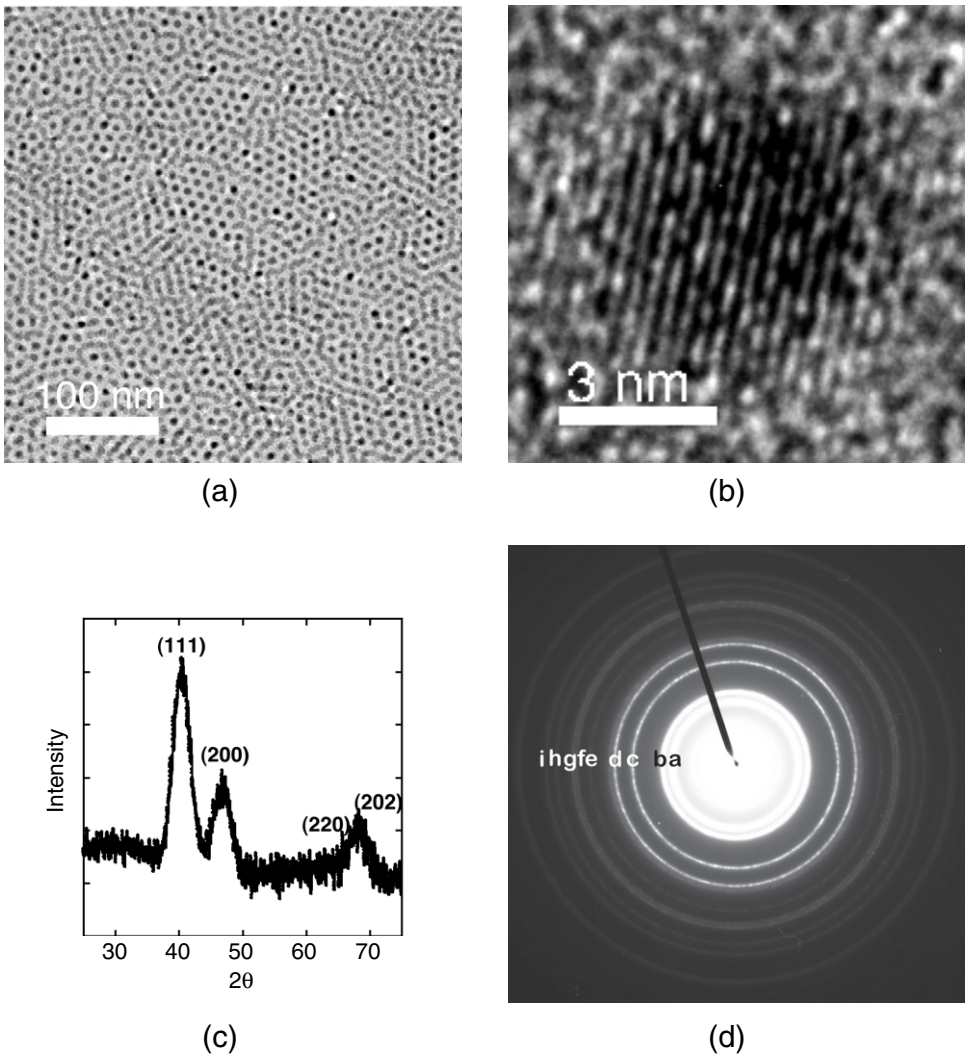

Figure 1. A bright field transmission electron micrograph of as-synthesized 6 nm $Fe_{27}Pt_{73}$ particles is shown in (a). The lattice planes are evident in a high resolution TEM (b) of a single 6 nm $Fe_{27}Pt_{73}$ particle, illustrating the crystalline nature of individual particles. (c) XRD and (d) SAD show the FCC nature of particles. Labels correspond to the following indices: a (111); b (200); c (220); d (311); e (400); f (331); g (420); h (422) and i (333).

all experiments $t = 0$ when the applied field is at maximum amplitude in order to account for the variations in quench time. The variations in quench time were less than 1% of the total time of the experiment. This experiment was also performed with other field strengths (either 100, 500 or 5000 Oe) for the 4C18 sample.

A series of magnetization decay curves at different temperatures for 6C18 are shown in figure 3. Similar results were seen for 4C18 [13] and 4C8. We assume that the time dependence t of the magnetization, M, or specific magnetization, σ, of a system at temperature T in these experiments can be described by the relation [11]

$$\sigma(H, t) = \sigma_0(H) - S(H)\ln(t - t'), \tag{1}$$

where $S(H)$, $\sigma_0(H)$ and t' are experimentally determined. The energy barrier distribution for the system can be extracted following the method of Gaunt [19, 20] and St Pierre *et al* [12]. Using equation (1) the magnetic viscosity parameter, S can be found at T. The energy barrier distribution is given by S/kT versus kT. Figure 4 shows S versus T (a) and energy barrier distributions (b) for samples 4C18, 4C8 and 6C18. $S(T)$ have been previously reported for 4C18 [13].

Figure 4 shows S to have a bimodel distribution. The low temperature region leads to an exponential component of the energy barrier distribution, while the higher temperature peak is responsible for a log normal distribution. For 4C18, 4C8 and 6C18 the higher temperature peak dominates $S(T)$ because magnetic contribution due to reversal is the largest contributor to S. The temperature at which this maxima occurs for each sample is 11 K for 4C18, 9 K for 4C8 and 19 K for 6C18. The low temperature region for 4C8 and 4C18 consists of a monotonic decay of S to zero for temperatures less than 4 K (4C18) and 3 K (4C8). However, for 6C18 the low temperature region is seen as a distinctive peak, with a maximum at around 5.5 K. The intensity of this region is much larger than for 4C18 and 4C8. No such change in intensity is seen for the higher temperature peak.

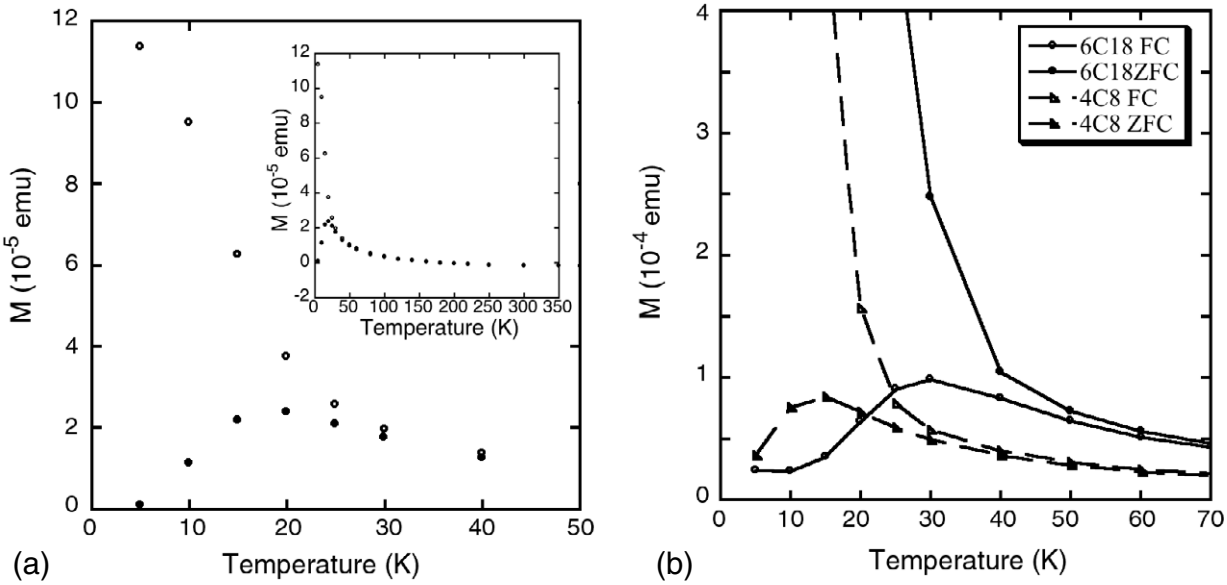

Figure 2. The T_B region of the ZFC and FC magnetization curve as a function of temperature for 4C18 in (a) where FC data is shown as open circles and ZFC as filled circles. The inset shows the full curves. (b) The blocking region for 6C18 and 4C8.

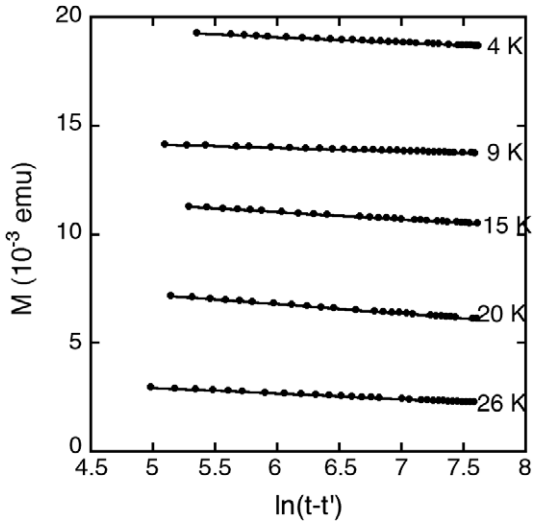

Figure 3. Magnetization measurements for sample 6C18 plotted as a function of $\ln(t - t')$. The time t is measured from the time of maximum applied field and t' is determined experimentally.

The energy barrier obtained from $S(T)$ can be seen in figure 4(b). It has two component distributions: a log normal and exponential. The form of these distributions has been given previously for ferritin by St Pierre *et al* [12]. For our FePt system the energy barrier distribution was also found to have this form, the fit is shown in figure 4(b). At low temperatures the exponential function dominates the particle dynamics. The changes in position of these components to the energy barrier correspond to the changes in S for both the low temperature region and high temperature maxima.

The effect of field on the energy barrier distribution was investigated by performing the previously described ZFC magnetic relaxation experiments with 100, 500 and 5000 Oe applied to the 4C18 particles. As before the field was applied and removed in order to create a magnetization at the start of the viscosity measurement. A comparison of the energy barriers attained for these and the original 7 T experiment are shown in figure 5(a), with S versus T given as an inset. In addition the ZFC and FC hysteresis measurements at 5 K are shown in (b) to give an idea of the magnetic state the system is in at a particular applied field. Demagnetization of the sample is seen at high fields.

In figure 5(a) it can be seen that as applied field decreases there is a loss in the low temperature exponential contribution and a shift in the maxima of the log normal distribution to lower temperatures. The maxima appears to have a field dependence. When fields greater than 5000 Oe are applied the maximum is centered on 1.3×10^{-22} J while at lower fields it is centered at 1×10^{-22} J. This dependence is more evident in the S versus T data where there is a shift of the higher temperature peak by a few Kelvin. As the applied field is reduced there is a decrease and eventual loss of the exponential component of the energy barrier. For fields less than 500 Oe the energy barrier distribution approaches zero and at 5000 Oe (a non-saturating field but larger than H_c) the energy barrier distribution at low fields no longer has an exponential component but tends to a constant finite value. At larger fields (certainly for $H \geqslant M_s$) the exponential contribution appears.

An alternate method for analysis of magnetic viscosity can be given in terms of activation rates as opposed to energy barriers. In this method $\sigma(t)$ has the form [13]

$$\sigma(t - t') \cong A(\alpha!) \frac{\alpha \tau_0^{\alpha}}{2^{\alpha}(t - t')^{\alpha}}, \tag{2}$$

where α, $A(\alpha!)$, t' and τ_0^{α} are found experimentally. This defines thermal reversal of an ensemble of spins over a period of time t in terms of rates τ_0. This relation is derived in the appendix and related to the energy barrier distribution determination described by Gaunt [19, 20].

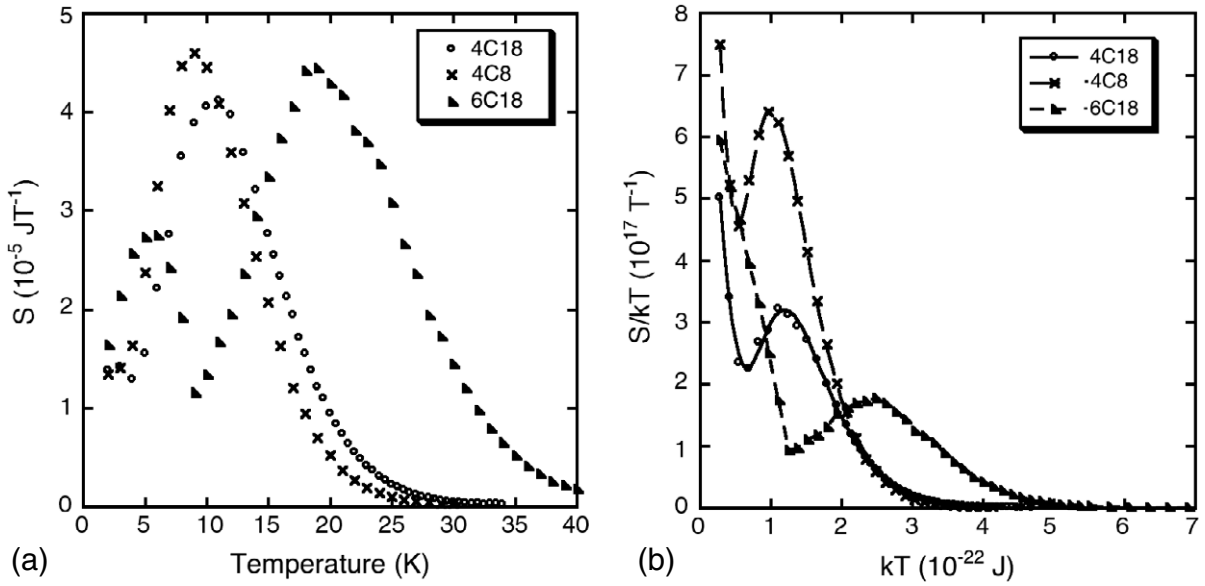

Figure 4. Magnetization measurements for sample 4C18, 4C8 and 6C18 (a) plotted as a function of $\ln(t - t')$. The time is measured from the time of maximum applied field and t' is determined experimentally. The energy barrier distributions for 4C18, 4C8 and 6C18 (b), the experimental data is shown as markers and the fit as a line.

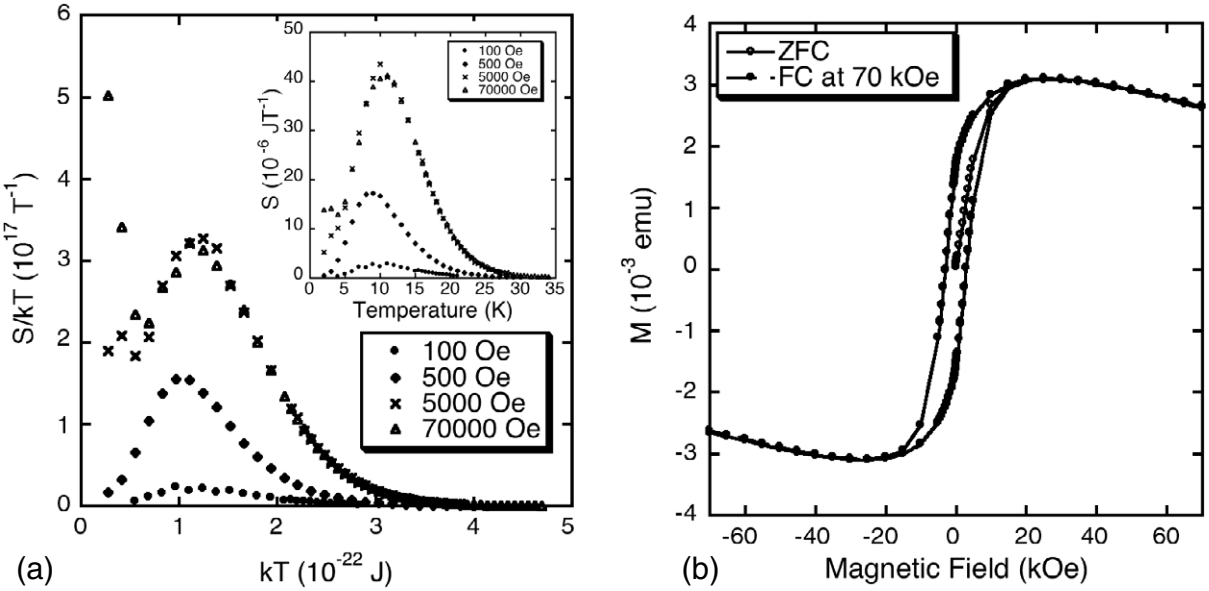

Figure 5. The energy barrier distribution (a) for 4C18 with different applied fields used to create an average moment. The inset shows the S versus T data for the same experiments. (b) 5 K hysteresis behavior of 4C18.

The exponent α in our rate distribution method provides important insight into the nature of slow dynamics. If $1 < \alpha < 2$, the distribution of relaxation times is broad in the sense that the mean diverges. If $0 < \alpha < 1$ the mean and variance diverge. Using equation (2), $M(t)$ data for 4C18, 4C8 and 6C18 was examined and results for α as a function of T are shown in figure 6. At low T for the 4C18 and 4C8 systems the exponent appears to be independent of temperature. For the 6C18 particles there is a distinctive peak in this low temperature region. Above these temperatures and below T_B for each sample there is a range were $\alpha \sim T$. One can show that this is expected for narrow barrier distributions. There is a maxima α for each sample at higher temperatures. 4C8 maxima is seen to be lower than 4C18 which is significantly lower than the 6C18 system. For all systems α is less than 1, indicating a broad distribution of relaxation times. α is smallest and the corresponding distribution widest at temperatures where the exponential component to the barrier distribution is largest. A consequence of this value for α is that components of the system can not relax on any timescale.

2.2.3. Ageing. Dynamic time wait experiments were performed in order to study the long time approach to equilibrium.

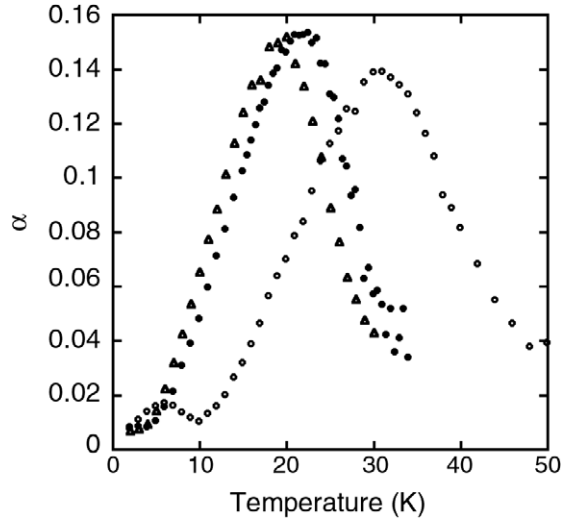

Figure 6. $M(t)$ fitted in terms of α as a function of temperature for 4C18 (solid circles), 4C8 (open triangles) and 6C18 (open circles).

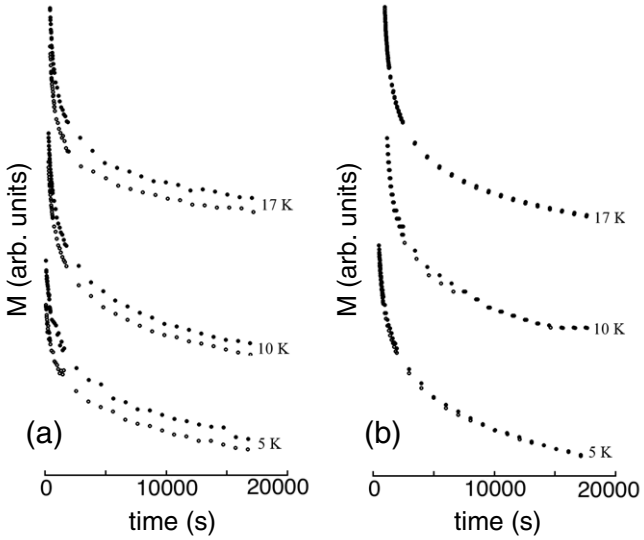

Figure 7. For sample 4C18 the sample is field cooled in 5 Oe (a) to 5, 10 or 17 K. (b) The sample is field cooled in 7 T to 5, 10 or 17 K. The upper curve for each temperature (solid circles) is for 10 000 s t_w, while the lower curve (open circles) has a 100 s t_w.

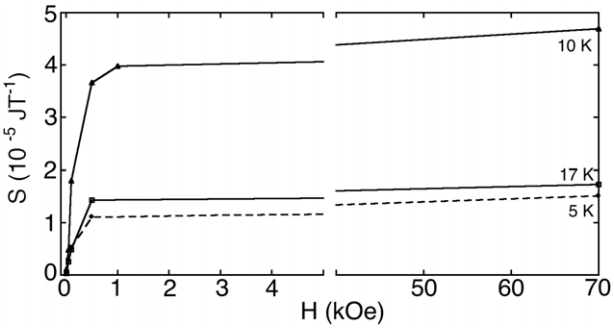

Figure 8. S versus H from FC 10 000 s t_w experiments for 4C18 at a given T.

History effects were studied using two different waiting times, t_w. Firstly FC experiments will be discussed, these experiments are similar to thermoremanent magnetization (TRM) but include monitoring of a waiting time. The sample is FC from above T_B to a desired temperature (either 5, 10, 17 K) in an applied field, H (either 5, 50, 100, 500, 1000 or 70 000 Oe). The sample was then left in a field for a t_w of 100 or 10 000 s. The field was then removed and the magnetization monitored for 10^4 s. These measurements were only performed on sample 4C18.

For 4C18 regardless of temperature, the time change of M did not appear to reach an asymptotic value when fields less than or equal to 100 Oe were applied. An equilibrium, defined as a stationary value of M, was reached for fields greater than 500 Oe. Example results are shown in figure 7. In (a) 5 Oe was applied and 4C18 was cooled to 5, 10 or 17 K and the system approached different final states depending on t_w. This may be an indication of ageing, when the system does not reach equilibrium in time. In (b) 4C18 was cooled in 7 T to 5, 10 or 17 K and the two different t_w measurements begin and decay into the same state, implying that the system reaches equilibrium.

Using equation (1) a value for S was found for the FC t_w experiments. This is given as a function of H and shown in figure 8 for $t_w \sim 10\,000$ s (similar results were attained for $t_w \sim 100$ s). Regardless of temperature or t_w there is a critical field at which ageing occurs: namely, $H \leqslant 100$ Oe. S is relatively constant at higher applied fields and there is only a slight increase as field increases due to the larger moment as the sample becomes more saturated.

ZFC time wait ageing experiments were also conducted. These experiments are similar to isothermal remanence magnetization (IRM), but include monitoring of a waiting time. These were performed on the 4C8, 4C18 and 6C18 systems. In these experiments the sample was cooled from above the T_B in zero field to a desired temperature (4–17 K). The sample was then left for either 100 or 5000 s. A 30 Oe field was then applied and subsequently removed and the magnets were quenched to ensure trapped flux was removed. The decay of the magnetic moment was subsequently monitored for approximately 16.5×10^4 s. Sample results at 6 and 7 K for 4C18 are shown in figure 9. For all temperatures and samples the initial states created by different waiting times either decayed to the same state (implying thermal equilibrium) or different states (implying non-equilibrium dynamics). The temperature at which ageing occurs is sample dependent. It was found that ageing occurred at $T \leqslant 4$ K for 4C8, $T \leqslant 6$ K for 4C18 and at $T \leqslant 8$ K for 6C18, while for higher temperatures ageing was not observed.

3. Discussion

The main focus of this work is to explore the nature and origin of the apparent exponential contribution to the reversal energy barrier for the FePt first seen by us in an earlier study [13] and later by others [14]. This contribution has also been seen previously in horse spleen ferritin [12] where

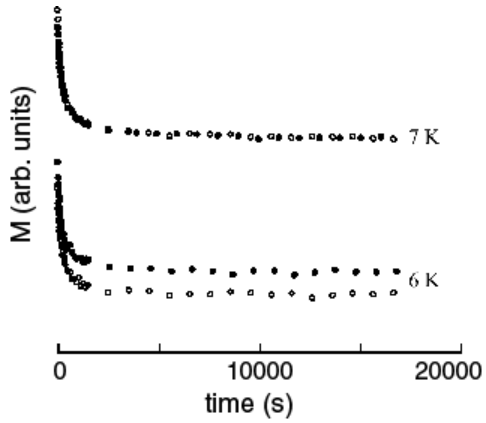

Figure 9. ZFC time wait experiments for 4C18 show that at 6 K ageing is present in the sample while at 7 K ageing no longer occurs. The upper curve (solid circles) for each temperature is for a 100 s time wait, while the lower curve (open circles) is for a 5000 s time wait.

it is postulated that the distribution results from the existence of multiple interacting magnetic entities within each particle. Kodama *et al* [15] showed an energy barrier distribution which diverges from zero energy using atomic scale modeling of ferrimagnetic nanoparticles with a surface roughness. Studies of nanocrystalline hexagonal ferrite [22] found a minor low temperature contribution to the energy barrier distribution in addition to the major component. They attributed its presence to weak demagnetizing interactions between the particles. Since no clear conclusions in the literature about the nature of this low temperature behavior exist, we have attempted to provide further understanding through detailed magnetic relaxation experiments on a range of particle systems that include a different surfactant matrix (4C8 and 4C18) as well as particles of different size (6C18 and 4C18).

The composition of samples used in this experiment approximate $FePt_3$. The possible effect of composition on our results compared with experiments on equiatomic FePt must be considered. Pt rich alloys have a topmost (111) layer containing exclusively Pt. For Fe alloys of Pt the subsequent second and third layers are found to decrease monotonously in concentration [23, 24]. This segregation of platinum occurs for ordered systems. Regardless of composition, all as-synthesised FePt systems were found to have an disordered γ phase from XRD [21]. Since our system is unordered like the equiatomic FePt, there should be no tendency for Pt segregation in the lattice. The composition of our particles may allow for the existence of an antiferromagnetic phase. However antiferromagnetism is only found in chemically ordered cubic $L1_2$ $FePt_3$ [25]. Since XRD (see figure 1(c)) confirmed the particles exist in the unordered FCC chemically disordered phase, we expect the system must be ferromagnetic below T_B [25, 26]. This is indeed what our magnetization measurements suggest and there is no evidence from $M(T)$ measurements for antiferromagnetic ordering.

It has been previously reported by Zhang *et al* [29] for Fe_2O_3 nanoparticles that the particle matrix effects magnetic relaxation, however this was not investigated in terms of energy barriers. The effect of the interparticle matrix on relaxation was explored in the present work by modification of the surfactant from the 18 carbon backbone (4C18) to the shorter 8 carbon backbone (4C8). Effects were not observed directly in the ZFC-FC curves (figure 2) of the samples. It is postulated that since T_B occurs over a range of temperatures the change in spacing, which is of the order of a few Angstroms, will not be significant enough to impact the experiments.

The effect of surfactant is more easily observed in viscosity measurements. In figure 4 the high temperature maxima of S and the low temperature region of S for 4C8 is shifted to lower temperatures compared to 4C18. Similarly both the log normal and exponential components of the energy barrier distribution (figure 4(b)) and the maxima in the α distribution (figure 6) are also shifted to lower values of T. Like Fe_2O_3 [29], the FePt matrix plays a role in determining the physical properties of the nanoparticles. The shift in the energy barrier to lower temperature when the surfactant matrix is changed suggests that the shorter carbon chained surfactants may affect the relaxation or enhance interparticle interactions, thus lowering the temperature for which blocking against thermal fluctuation occurs (on the timescale of the measurement). We are thus left with the possibility that the matrix itself mediates interactions or otherwise affects relaxation rates.

The 6C18 system has the same surfactant matrix as 4C18 particles, thus in this regards should have similar behavior [30]. Although both the 6C18 and 4C18 particles have the same surfactant matrix, the 6C18 are larger and spaced slightly farther apart than the 4C18. The increase in size of the 6C18 particles compared to 4C18 particles results in an increase in thermal activation energy. This is evident by the shift of T_B (figure 2) by about 15 K for 6C18 compared to 4C18. Furthermore, we see a large shift in the peak maxima of $S(T)$, the energy barrier distribution and $\alpha(T)$ associated with reversal (figures 4 and 6). There is only a small shift in the maxima or region associated with the low temperature behavior of $S(T)$, the energy barrier distribution and $\alpha(T)$.

The intensity of the peaks in the distributions shown in figures 4 and 6 must also be considered. There is no significant increase in the intensity of the high temperature maxima governed by reversal with the increase in particle size from 4 to 6 nm. However, in the low temperature region we see a large increase in intensity of the maximum for 6C18 compared to 4C18 and 4C8. The discrepancy in both temperature shift and change in intensity of the maxima in the low temperature and high temperature regions of $S(T)$, the energy barrier distribution and $\alpha(T)$ suggest that different processes govern the behavior in these temperature regions. We conclude that increasing particle size changes the temperature at which magnetic reversal occurs, but does not affect the low temperature behavior in the same manner.

The increase in the exponential component to the energy barrier distribution for 6C18 compared to 4C18 may be due to a change in the interaction energy between neighboring particles. The 6C18 particles are larger than the 4C18 and might therefore generate stronger stray magnetic fields simply due to having larger moments. Interactions between FePt

nanoparticles have been previously calculated as an energy product $(BH)_{max}$ [31]. Since the FePt particles are generally monodispersed (the exception was 6C18 which had a 5% contribution of 3 nm particles) and have a given interparticle separation determined through self assembly, a value for the interaction between neighboring particles can be found using the Aharoni relation for the magnetic interaction between spheres [32]. The average induced field from nearest neighbors is given by

$$\langle H_z \rangle = \frac{4\pi M}{3}\left(\frac{R_1}{R_0}\right)^3 (3\cos^2\Theta_0 - 1), \qquad (3)$$

where H_z is the average field, M the magnetization, R_1 the particle radius, R_0 the distance between the two particles' centers and Θ_0 the angle between particles. The values for these are found from TEM and are given in table 1.

M for both samples was found as follows. The volume of a single FCC unit cell was calculated by using the lattice parameters obtained from XRD and SAD taking into account that $a \neq c$, so $V_{FCC} = a^2c$ [18]. The number of atoms, N_{atoms}, in a particle is thus $4P(V_{particle}/V_{FCC})$, where P is the atomic packing factor (P for an FCC unit is 0.74), 4 is the number of atoms in an FCC unit cell and $V_{particle}$ is the volume of a particle given by $\frac{4\pi R_1^3}{3}$. Using the composition for each system the number of Fe atoms, N_{Fe} for each is found.

The magnetic moment, μ_{Fe} of a single atom was taken as 0.8 μ_B for 4C18 and 1 μ_B for 6C18 [33, 34]. These values are for bulk FePt alloys and it should be noted that Robach *et al* [27] found that the moment of Pt for non-equiatomic FePt films is significantly less that that from the bulk alloy. So the effect of Pt on these measurements may be less than our estimate. This calculation however, is meant to only provide an estimation of possible particle interactions due to magnetic field. More detailed methods are found elsewhere [28].

The moment for the whole particle, $\mu_{particle}$ is given by the $\mu_{Fe}N_{Fe}$ and the magnetization is $M = \mu_{particle}\frac{4\pi R_1^3}{3}$. An effective field acting on a particle can then be calculated and an estimate made for the dipolar energy E for each interacting pair. The corresponding temperature is given by E/k_B. Results for 6C18 and 4C18 are shown in table 1. For both systems there appears to be interaction strengths at temperatures reminiscent of the exponential contribution to the energy barrier distributions seen in figure 4(b).

The energy barrier distributions which result from static viscosity measurements with different initial fields (see figure 5) display two features. A loss of the exponential contribution and a shift of the log normal component to lower temperatures when small applied fields are used. The absence of the low energy barrier distribution in small applied field is consistent with the existence of interparticle dipolar interactions. Effects from interactions are not seen when small fields are applied because the thermally driven reversals require only low energies and the system is likely to have relaxed before measurements can be made at accessible temperatures. When more magnetic moments are magnetized using a large field, not all moments relax before measurements are made and an additional component to the viscosity is observed.

Table 1. Parameters calculated for interaction potential.

	4C18	6C18
R_1 (nm)	2	3
R_0 (nm)	6.8	9.9
N_{atoms}	1460	4900
N_{Fe}	290	1330
M (A m^{-1})	6.5×10^4	1×10^5
H_z (A m^{-1})	1.6×10^5	2.8×10^5
E (J)	3.4×10^{-23}	3.4×10^{-22}
T (K)	2.5	25

We postulate that this additional component appears as an exponential contribution to the energy barrier distribution when analyzed in terms of magnetic viscosity.

If the exponential contribution to the energy barrier is due to long-range dipolar interactions then the FC curves might be expected to flatten below T_B (e.g. Parker *et al* [5]). This is not seen in figure 2. However, one must take into account the timescale of the measurement. It is possible that interactions lead to equilibration before the magnetization measurement is made by the SQUID magnetometer. Typical times for a SQUID magnetometer are 15 s. Stahl *et al* [35] obtained magnetization curves for FePt on a VSM with much faster measurement times (1 s). Their experiments show a FC magnetization curve which tends to flatten as T approaches zero. This is what would be expected for an interacting particle system.

The above considerations are consistent with features identified when the analysis is made using a rate distribution characterized by exponent α. Using activation rates to obtain a distribution of relaxation times, one expects that $\alpha \sim T$ (see the appendix for details). But this is only seen for temperatures below the blocking temperature and above 5 K (4C18 and 4C8) or 10 K (6C18). The exponent has a maximum near the blocking temperature and appears to be independent of temperature below 5 K (4C18 and 4C8) or 10 K (6C18). At these low temperatures α is less than 1 indicating a broad distribution of relaxation energies. Equations of the form shown in equation (2) have long been associated with statistical changes governed by rare events and nonmagnetic glasses [36]. We conclude that there are a large number of processes at low T, with a non-negligible 'tail' corresponding to the existence of rare events on all timescales.

If the above argument for the existence of weak interactions is correct, then there may be measurable correlation effects due to long-range coupling between magnetic particles. Observation of these correlation effects depends on the temperature and most importantly, the time over which a measurement is made. At low temperatures, weak interactions leading to long-range correlations between particles may be observed on long timescales. At higher temperatures, these effects may disappear rapidly and not be visible in quasi-static measurements.

There is an interesting caveat to the high temperature disappearance of measurable correlations if the distribution of relaxation times is broad. The significance of a distribution with a power law exponent in the 'broad' range, as described above, is that there exists nonzero probability of rare events which are measurable. The effect from rare events is exactly

what is probed in an ageing experiment. Even if the majority of events occur on short timescales there are still events affecting long time evolution.

4. Conclusion

Previously, Gorham *et al* [39] found that these broad distributions exist in interacting spin glass systems and affect the energy landscape of the system. Our suggestion is that the exponential contribution to the energy barrier distribution may at least be partially the consequence of weak interactions between particles. Thus the reversal events responsible for the exponential contribution to the measured viscosity are visible at low temperatures over times on the order of seconds. Because the distribution of relaxation times associated with these interactions is broad, there also exist events associated with the weak interaction that occur infrequently but have large, measurable consequences. These are what are observed in ageing. These events are essentially large Barkhausen events where the participating particles are correlated via magnetostatic stray fields, and also possibly affected by the nonmagnetic matrix.

Relaxation experiments performed on interacting spin glass systems are know to be dependent on the waiting time for quenched states [4, 37]. However non-interacting superparamagnetic or dilute weakly interacting systems exhibit no such dependence [38]. In these cases particle size distribution could effect ageing seen in both FC and ZFC experiments. However the deviation of our as-synthesised FePt was small (5–7.5%), so distribution of size should have minimal effect. The temperatures at which ageing in our ZFC experiments was seen correspond to those of the exponential contribution to the energy barrier. For the 6C18 particles we have seen an increase in the low temperature maxima of $S(T)$ as well as ageing at higher temperatures than 4C18 and 4C8. This suggests that ageing and viscosity in our particles may be affected by particle size in addition to long-range interaction effects. Since 4C8 does not age over the same temperature range as 4C18 it is possible that surfactant also plays some role in these observed features.

In the FC ageing experiments shown in figure 7, we see a temperature independence for ageing when measurements were performed with a field $\leqslant$100 Oe. At fields greater than 100 Oe no ageing was seen. This may be a consequence of the experimental and timescales. The sample cooled in field is supplied with additional energy compared to ZFC experiments allowing the possibility of ageing at higher temperatures through creation of metastable states. The field dependence of the ageing experiments seen in figure 8 has been observed previously for Fe_3O_4 particles [40]. Both the FePt and Fe_3O_4 particles FC magnetization curves show a peak at some field. El-Hilo *et al* [40] showed this phenomenon results from the time dependence of the measurement. They observed that the peak only developed after 15 s. All measurements we made for FePt had $t > 15$ s so a peak would be expected and was in fact observed. Thus the ageing seen in both FC and ZFC cooled experiments further supports the possibility that rare events associated with broad rate distributions are occurring over long timescales.

In summary, we have attempted to understand an exponential component to energy barrier distributions reported in a number of systems [12–14]. We found that matrix effects and interparticle interactions seem to play a role in magnetic reversal of FePt particles as well as time dynamics of the experiments. In particular, shortening the surfactants reduces the viscosity. Increasing particle size affects the low temperature components of $S(T)$, the energy barrier distribution and α differently to the reversal peak contribution at higher temperatures, suggesting that perhaps this region is not as strongly governed by thermal activation energy as the reversal region. The broadness of the α distribution and the ageing seen in time wait experiments are symptomatic of interparticle interaction. Finally we have also introduced a method of quantifying relaxation in terms of relaxation rates and exponents useful for characterizing long time dynamics.

Acknowledgments

The authors are grateful for the support of the Australian Research Council and Seagate Technology as well as the technical assistance of Dr Martin Saunders and Dr Robert C Woodward. R O Fuller was the holder of an Australian Postgraduate Award.

Appendix

The broadness of the relaxation rate distribution in FePt is suggested by the slower than exponential time dependence of magnetic relaxation, the dependence of the critical barrier on measurement timescale and the width of the energy distribution being larger than kT. In earlier work a general broad distribution was found to fit magnetic viscosity data of the particulate systems [13]. The time dependence of magnetization was given in terms of activation rates as opposed to energy barriers and will be derived in full here.

A.1. Time distribution

If $\tau_\uparrow$ and $\tau_\downarrow$ represent the random times the particles spend in the $\uparrow$ and $\downarrow$ states and these states are separated by a barrier of defined energy $\Delta E_\uparrow$. The mean jump time $\overline{\tau_\uparrow}$ is given by the Arrhenius–Néel law:

$$\overline{\tau}_\uparrow = \tau_{0\uparrow} e^{\Delta E_\uparrow/(kT)}, \tag{A.1}$$

where $\tau_{0\uparrow}$ is a constant, k is the Boltzmann constant and T is the temperature. For a given barrier height

$$P(\tau_\uparrow|\overline{\tau}_\uparrow) = \frac{1}{\overline{\tau}_\uparrow} e^{-\tau_\uparrow/\overline{\tau}_\uparrow}. \tag{A.2}$$

The distribution of $\overline{\tau_\uparrow}$ is

$$P(\overline{\tau}_\uparrow) = P(\Delta E_\uparrow) \left| \frac{\mathrm{d}\Delta E_\uparrow}{\mathrm{d}\overline{\tau}_\uparrow} \right|, \tag{A.3}$$

where $P(\Delta E_\uparrow)$ is the distribution of barriers. The distribution of jump times is

$$P_\uparrow(\tau_\uparrow) = \int_0^\infty P(\tau_\uparrow|\overline{\tau}_\uparrow)P(\overline{\tau}_\uparrow)\,\mathrm{d}\overline{\tau}_\uparrow. \tag{A.4}$$

For the special case of exponentially distributed barriers we can assume that $P(\Delta E_\uparrow)$ has the form

$$P(\Delta E_\uparrow) = \frac{1}{\Delta E_{0\uparrow}}\mathrm{e}^{-\Delta E_\uparrow/\Delta E_{0\uparrow}}. \tag{A.5}$$

Since equation (A.1) has $\mathrm{d}\Delta E_\uparrow/\mathrm{d}\overline{\tau}_\uparrow = kT/\overline{\tau}_\uparrow$ then we can introduce $\alpha_\uparrow = kT/\Delta E_{0\uparrow}$ then equation (A.3) becomes

$$P(\overline{\tau}_\uparrow) = \alpha_\uparrow \frac{\tau_{0\uparrow}^{\alpha_\uparrow}}{\overline{\tau}_\uparrow^{1+\alpha_\uparrow}} \tag{A.6}$$

this is a Pareto distribution. Using (A.4) and letting $y = \tau_\uparrow/\overline{\tau}_\uparrow$ then

$$P_\uparrow(\tau_\uparrow) = \alpha_\uparrow \tau_{0\uparrow}^{\alpha_\uparrow} \int_0^{\tau_\uparrow/\tau_{0\uparrow}} \mathrm{d}y\, y^{\alpha_\uparrow}\mathrm{e}^{-y} \tag{A.7}$$

this is an incomplete Gamma distribution which has the exact solution

$$P_\uparrow(\tau_\uparrow) = \alpha_\uparrow \frac{\tau_{0\uparrow}^{\alpha_\uparrow}}{\tau_\uparrow^{1+\alpha_\uparrow}} \gamma\left(1+\alpha_\uparrow, \frac{\tau_\uparrow}{\tau_{0\uparrow}}\right). \tag{A.8}$$

At long times $\gamma(1+\alpha_\uparrow, \frac{\tau_\uparrow}{\tau_{0\uparrow}}) \to \Gamma(1+\alpha_\uparrow) = \alpha_\uparrow\Gamma(\alpha_\uparrow)$ thus

$$P_\uparrow(\tau_\uparrow) \simeq \alpha_\uparrow^2\Gamma(\alpha) \frac{\tau_{0\uparrow}^{\alpha_\uparrow}}{\tau_\uparrow^{1+\alpha_\uparrow}} \tag{A.9}$$

if $\alpha_\uparrow$ is small enough there is a Lévy flight on the time axis.

A.2. Rate equations

If $\pi_\uparrow(t)$ and $\pi_\downarrow(t)$ denote the populations of the up and down state and $\pi_\uparrow(t) + \pi_\downarrow(t) = 1$ and $\pi_\uparrow(0) = 1$ if the sample is fully magnetized. Then from rate equations

$$\dot{\pi}_\uparrow = -\Gamma\pi_\uparrow + \Gamma\pi_\downarrow \tag{A.10}$$

$$\dot{\pi}_\downarrow = +\Gamma\pi_\uparrow - \Gamma\pi_\downarrow. \tag{A.11}$$

Simple calculations lead to

$$\pi_\uparrow(t) = \tfrac{1}{2}(1+\mathrm{e}^{-2\Gamma t}). \tag{A.12}$$

The magnetic moment $\sigma_\Gamma(t)$ is given as

$$\sigma_\Gamma(t) = A(\pi_\uparrow(t) - \pi_\downarrow(t)) = A(2\pi_\uparrow(t) - 1) = A\mathrm{e}^{-2\Gamma t} \tag{A.13}$$

where A is a constant, Γ in $\sigma_\Gamma(t)$ is different for each particle. What is observed is an ensemble average $\bar{\sigma}(t)$ of $\sigma_\Gamma(t)$

$$\bar{\sigma}(t) \equiv \int_0^\infty \mathrm{d}\Gamma\, P(\Gamma)\sigma_\Gamma(t) \tag{A.14}$$

this derivation is valid for any barrier.

If we specifically take the exponential equation (A.5) then the jump rate Γ is the reciprocal of the mean jump time $\overline{\tau}_\uparrow = \overline{\tau}_\downarrow$ (in no applied field). Thus with equation (A.1) Γ is

$$\Gamma = \tau_{0\uparrow}^{-1}\mathrm{e}^{-\Delta E_\uparrow/(kT)}. \tag{A.15}$$

Using this with $P(\Gamma) = P(\Delta E_\uparrow)|\mathrm{d}\Delta E_\uparrow/\mathrm{d}\Gamma|$ for $0 < \Gamma < \tau_{0\uparrow}^{-1}$ then $\overline{\sigma}(t)$ is

$$\overline{\sigma}(t) = A\frac{\alpha_\uparrow\tau_{0\uparrow}^{\alpha_\uparrow}}{(2t)^{\alpha_\uparrow}}\Gamma(\alpha_\uparrow, 2t/\tau_{0\uparrow}). \tag{A.16}$$

For long times when $2t/\tau_{0\uparrow} \gg 1$ a power law is obtained

$$\overline{\sigma}(t) = A\Gamma(\alpha_\uparrow)\frac{\alpha_\uparrow\tau_{0\uparrow}^{\alpha_\uparrow}}{(2t)^{\alpha_\uparrow}}. \tag{A.17}$$

When the exponential relaxation $\sigma_\Gamma(t)$ of equation (A.13) for a given Γ into an ensemble of average $\overline{\sigma}(t)$ of equation (A.4) then

$$\overline{\sigma}(t) = A\int_0^\infty \mathrm{d}\Gamma\, P(\Gamma)\mathrm{e}^{-2\Gamma t}. \tag{A.18}$$

References

[1] Jönsson P E 2004 Superparamagnetism and spin glass dynamics of interacting magnetic nanoparticles *Adv. Chem. Phys.* **128** 191

[2] Dorman J L, Fiorani D and Tronc E 1997 Magnetic relaxation in fine-particle systems *Adv. Chem. Phys.* **98** 283

[3] Lundgren L, Svedlindh P, Norblad P and Beckman O 1983 Dynamics of the relaxation-time spectrum in CuMn spin-glass *Phys. Rev. Lett.* **51** 911

[4] Jonsson T, Mattsson J, Djurberg C, Khan F A, Nordblah P and Svendlin P 1995 Aging in a magnetic particle system *Phys. Rev. Lett.* **75** 4138

[5] Parker D, Ladieu F, Vincent E, Mériguet G, Dubois D, Dupuis V and Perzynski R 2005 Experimental investigation of superspin glass dynamics *J. Appl. Phys.* **97** 10A502

[6] Kundu A K, Norblad P and Rao C N R 2005 Nonequilibrium magnetic properties of single-crystalline $La_{0.7}Ca_{0.3}CoO_3$ *Phys. Rev.* B **72** 144423

[7] Cugliandolo L F and Kurchan J 1993 Analytical solution of the off-equilibrium dynamics of long-range spin-glass model *Phys. Rev. Lett.* **71** 173

[8] Berthier L and Bouchaud J-P 2002 Geometrical aspects of aging and rejuvenation in the Ising spin glass: a numerical study *Phys. Rev.* B **66** 054404

[9] Sasaki M, Jönsson P E, Takayama H and Mamiya H 2005 Aging and memory effects in superparamagnets and superspin glasses *Phys. Rev.* B **71** 104405

[10] Charkraverty S, Bandyopadhyay M, Chatterjee S, Dattagupta S, Frydman A, Sengupta S and Sreeram P A 2005 Memory in a magnetic nanoparticle system: polydispersity and interaction effects *Phys. Rev.* B **71** 054401

[11] Street R and Woolley J C 1949 A study of magnetic viscosity *Proc. Phys. Soc. Lond.* A **52** 562

[12] St Pierre T G, Gorham N T and Allen P D 2001 Apparent magnetic energy-barrier distribution in horse-spleen ferritin: evidence for multiple interacting magnetic entities per ferrihydrite nanoparticle *Phys. Rev.* B **65** 024426

[13] Fuller R O, Koutsantonis G A, Stamps R L and Bardou F 2005 Broad distributions of relaxation times in FePt nanoparticles *J. Appl. Phys.* **97** 10J508

[14] Gorham N T, Woodward R C, St Pierre T G, Terris B D and Sun S 2005 Apparent magnetic energy-barrier distribution in FePt nanoparticles *J. Magn. Magn. Mater.* **295** 174–6

[15] Kodama R H and Berkowitz A E 1999 Atomic-scale magnetic modeling of oxide nanoparticles *Phys. Rev.* B **59** 6321
[16] Mamiya H, Ohnuma M, Nakatani I and Furubayashi T 2006 New approach for magnetic relaxations in nanomagnet assemblies *Europhys. Lett.* **74** 500
[17] Sun S, Murray C B, Weller D, Folks L and Moser A 2000 Monodispersed FePt nanoparticles and ferromagnetic FePt nanocrystal superlattices *Science* **287** 1989
[18] Klemmer T J, Shukla N, Liu C, Wu X W, Svedberg E B, Mryasov O, Chantrell R W, Weller D, Tanase M and Laughlin D E 2002 Structural studies of $L1_0$ FePt nanoparticles *Appl. Phys. Lett.* **81** 2220
[19] Gaunt P 1976 Magnetic viscosity in ferromagnets I. Phenomenological theory *Phil. Mag.* **34** 775
[20] Gaunt P 1986 Magnetic viscosity and thermal activation energy *J. Appl. Phys.* **59** 4129
[21] Rong C-B, Li Y and Liu J P 2007 Curie temperatures of annealed FePt nanoparticle systems *J. Appl. Phys.* **101** 09K505
[22] Batlle X, García del Muro M and Labarta A 1997 Interaction effects and energy barrier distribution on the magnetic relaxation of nanocrystalline hexagonal ferrites *Phys. Rev.* B **55** 6440
[23] Beccat P, Gauthier Y, Baudoing-Savois R and Bertolini J C 1990 Monotonous concentration profile and reconstruction at $Pt_{80}Fe_{20}(111)$: LEED study of a catalyst *Surf. Sci.* **238** 105–18
[24] Creemers C and Deurinck P 1997 Platinum segregation to the (111) surface of ordered $Pt_{80}Fe_{20}$: LEIS results and model simulations *Surf. Interface Anal.* **25** 177–90
[25] Bacon G E and Crangle J 1963 Chemical and magnetic order in platinum rich Pr + Fe alloys *Proc. R. Soc.* A **272** 387
[26] White C W, Withrow S P, Sorge K D, Meldrum A, Budai J D, Thompson J R and Boatner L A 2003 Oriented ferromagnetic Fe–Pt alloy nanoparticles produced in Al_2O_3 by ion-beam synthesis *J. Appl. Phys.* **93** 5656
[27] Robach O, Quiros C, Valvisares S M, Walker C J and Ferrer S 2003 Structure and Pt magnetisim of FePt nanoparticles investigated with x-ray diffraction *J. Magn. Magn. Mater.* **264** 202
[28] Crew D C, Farrant S H, McCormick P G and Street R 1996 Measurement of magnetic viscosity in a Stoner–Wohlfarth material *J. Magn. Magn. Mater.* **163** 299
[29] Zhang X X, Ziolo R, Kroll E C, Bohigas X and Tejada J 1995 Magnetic relaxation and quantum tunneling in nanocrystalline particles *J. Magn. Magn. Mater.* **140–144** 1853
[30] Okamoto S, Kitakami O, Kikuchi N, Miyazaki T and Shimada Y 2003 Size dependence of magnetic properties and switching behavior in FePt $L1_0$ nanoparticles *Phys. Rev.* B **67** 094422
[31] Zeng H, Li J, Wang Z L, Liu J P and Sun S 2002 Interparticle interactions in annealed FePt nanoparticle assemblies *IEEE Trans. Magn.* **38** 2598
[32] Aharoni A 1987 Magnetic interaction between spheres *IEEE Trans. Magn.* **23** 1853
[33] Aboaf J A, McGuire T R, Herd S R and Klokholm E 1984 Magnetic, transport, and structural properties of iron–platinum thin films *IEEE Trans. Magn.* **20** 1642
[34] Men'shikov A Z, Dorofeyev Y A, Kazantsev V A and Sidorov S K 1974 Magnetic structure of ordered iron–platinum alloys *Fiz. Metal. Metalloved.* **38** 505
[35] Stahl B, Ellrich J, Theissmann R, Ghafari M, Bhattacharya S, Hahn H, Gajbhiye N S and Kramer D 2003 Electronic properties of 4 nm FePt particles *Phys. Rev.* B **67** 014422
[36] Donth E 2001 *The Glass Transition Relaxation Dynamics in Liquids and Disordered Materials* (Berlin: Springer)
[37] Refregier P, Vincent E, Hammann J and Ocio M 1987 Ageing phenomena in a spin-glass: effect of temperature changes below T_g *J. Physique* **48** 1533
[38] Tsoi G M, Wenger L E, Senaratne U, Tackett R J, Buc E C, Naik R, Vaishnava P P and Naik V 2005 Memory effects in a superparamagnetic γ-Fe_2O_3 system *Phys. Rev.* B **72** 014445
[39] Gorham N T, Woodward R C, St Pierre T G, Stamps R L, Walker M J, Greig D and Matthew J A D 2004 Experimental determination of Lévy flight distributions of the energy barriers in spin glasses *J. Appl. Phys.* **95** 6983
[40] El-Hilo M, O'Grady K and Popplewell J 1991 The peak in the TRM fine particle system *J. Appl. Phys.* **69** 5133